

See discussions, stats, and author profiles for this publication at: <https://www.researchgate.net/publication/264164386>

# Battery-Operated, Portable, and Flexible Air Microplasma Generation Device for Fabrication of Microfluidic Paper-Based Analytical Devices on Demand

ARTICLE *in* ANALYTICAL CHEMISTRY · JULY 2014

Impact Factor: 5.64 · DOI: 10.1021/ac501945q · Source: PubMed

---

CITATIONS

5

---

READS

87

## 2 AUTHORS:



Peng-Kai Kao

University of Michigan

10 PUBLICATIONS 48 CITATIONS

[SEE PROFILE](#)



Cheng-che Hsu

National Taiwan University

70 PUBLICATIONS 457 CITATIONS

[SEE PROFILE](#)

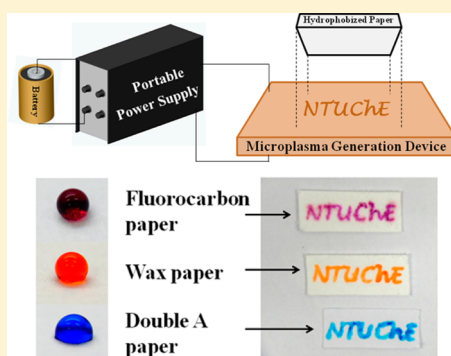
# Battery-Operated, Portable, and Flexible Air Microplasma Generation Device for Fabrication of Microfluidic Paper-Based Analytical Devices on Demand

Peng-Kai Kao and Cheng-Che Hsu\*

Department of Chemical Engineering, National Taiwan University, Taipei, 10617, Taiwan

 Supporting Information

**ABSTRACT:** A portable microplasma generation device (MGD) operated in ambient air is introduced for making a microfluidic paper-based analytical device ( $\mu$ PAD) that serves as a primary healthcare platform. By utilizing a printed circuit board fabrication process, a flexible and lightweight MGD can be fabricated within 30 min with ultra low-cost. This MGD can be driven by a portable power supply (less than two pounds), which can be powered using 12 V-batteries or ac-dc converters. This MGD is used to perform maskless patterning of hydrophilic patterns with sub-millimeter spatial resolution on hydrophobic paper substrates with good pattern transfer fidelity. Using this MGD to fabricate  $\mu$ PADs is demonstrated. With a proper design of the MGD electrode geometry,  $\mu$ PADs with 500- $\mu$ m-wide flow channels can be fabricated within 1 min and with a cost of less than \$USD 0.05/device. We then test the  $\mu$ PADs by performing quantitative colorimetric assay tests and establish a calibration curve for detection of glucose and nitrite. The results show a linear response to a glucose assay for 1–50 mM and a nitrite assay for 0.1–5 mM. The low cost, miniaturized, and portable MGD can be used to fabricate  $\mu$ PADs on demand, which is suitable for in-field diagnostic tests. We believe this concept brings impact to the field of biomedical analysis, environmental monitoring, and food safety survey.



Microfluidic paper-based analytical devices ( $\mu$ PADs) have recently gained significant attention for potential applications in general healthcare,<sup>1–4</sup> immunochemical assays,<sup>5</sup> biochemical analysis,<sup>6</sup> environmental monitoring,<sup>7,8</sup> and food safety.<sup>9</sup> For a  $\mu$ PAD, the paper substrate was patterned into regions of hydrophilic channels demarcated by hydrophobic barriers. Compared with conventional glass-based or polydimethylsiloxane-based microfluidics,  $\mu$ PADs are great candidates as point-of-care diagnostic tools with advantages of low cost, fast response, facile interpretation, simple disposal, and no pumps being required to transport the fluidics on a porous paper substrate due to capillary action.<sup>10</sup> A promising paper-based microfluidic device was first developed by the Whitesides group using the photolithography process.<sup>6</sup> Since that time, there has been a great number of literature reporting different fabrication techniques, such as plasma etching,<sup>11</sup> plasma polymerization,<sup>12</sup> wax printing,<sup>13,14</sup> inkjet printing,<sup>15</sup> contact printing,<sup>16</sup> flexographic printing,<sup>17</sup> plotting,<sup>18</sup> cutting,<sup>19</sup> and drawing.<sup>20</sup> Jet-type plasma sources<sup>21</sup> with an ultrathin nozzle can potentially be used for  $\mu$ PAD fabrication. Although several of the above processes offer advantages of low cost and possibility for large scale fabrication, it is required to manufacture the  $\mu$ PADs in the laboratory and then ship the devices to a designated location. For applications such as in-field diagnostics, fabrication of  $\mu$ PADs on site or on-demand offers great advantages. Under this circumstance, a facile and low-cost process that possesses good pattern transfer fidelity

and is operated using portable and battery-powered equipment is highly desired.

Atmospheric-pressure (AP) microplasmas<sup>22</sup> are plasmas operated under 1 atm with at least one geometric dimension confined to 1 mm or less. According to the “ $pd$  scaling” of the Paschen curve, a sufficiently small distance gap results in stable glow discharges generated by reasonably low applied voltage at 1 atm.<sup>22</sup> In addition, the miniaturized dimension offers a locally highly reactive environment with high power density but small total power consumption. These features enable AP microplasma to be utilized in various applications, such as maskless patterning,<sup>23,24</sup> biomedical applications,<sup>25</sup> optical spectroscopy, and mass spectrometry.<sup>26,27</sup> Due to their sub-millimeter miniaturized size, microplasma generation devices (MGDs) are most often fabricated using semiconductor fabrication processes such as lithographic and/or vacuum-based processes, which are expensive and time-consuming. Using a screen print-based process to fabricate MGDs has recently been reported.<sup>28</sup> This process offers advantages of low cost and high accessibility, but it requires several hours to fabricate a MGD. For the MGD to be utilized as a tool to fabricate  $\mu$ PADs, a low-cost and rapid process to fabricate MGDs is highly desired.

Among several types of AP microplasma systems reported in the literature,<sup>29,30</sup> dielectric barrier discharge (DBD) is one

Received: May 26, 2014

Accepted: July 23, 2014

Published: July 23, 2014



type that has been widely utilized. A DBD-type system consists of one or more dielectric layers located between two electrodes. The existence of the dielectric layer effectively prevents the formation of arc discharge and enables the formation of spatially uniform low temperature (near room temperature) plasmas with low power consumption. Based on these characteristics, DBDs have been widely employed in ozone generation, surface treatment, and gas decomposition or reforming.<sup>31,32</sup> In this work, we report the development of a low-cost DBD-type MGD that can be fabricated in a simple, efficient, and cost-effective manner. This MGD can be operated in ambient air and is battery powered. A facile and low cost process using this MGD to fabricate  $\mu$ PADs is demonstrated. Finally we test the  $\mu$ PADs by performing quantitative colorimetric assays and establish calibration charts for detection of glucose and nitrite. The impact using this portable MGD-based  $\mu$ PAD fabrication process in in-field diagnostic tests will be discussed.

## EXPERIMENTAL SECTION

**Fabrication of  $\mu$ PADs. AP MGD.** Figure 1A shows a photograph of the battery-operated, portable MGD. This system consists of a high-voltage ac power supply (PVM12, Information Unlimited, USA) and a MGD. The ac power source requires 12 V dc input, which can be either batteries (e.g., A23, Sony, as shown in this figure) or using an ac–dc converter. We note that the use of a 12 V battery to drive this ac power source offers great possibilities when the MGD is used in the field. For example, lead-acid rechargeable batteries for automobiles are able to deliver dc 12 V. A battery with a capacity of 45 amp-hour is sufficient to supply the MGD operation for at least 20 h. In this work, an ac–dc converter is used to fabricate the  $\mu$ PADs. The power source delivers ac voltages with a frequency between 20 and 50 kHz and a voltage up to 15 kV. We note that the amplitudes of the ac voltages reported in this work are all peak-to-peak voltages. The MGD is fabricated using a modified printed circuit process based on the toner transfer method. The fabrication process defines patterns on a double-sided copper clad laminate (CCL), with the detail illustrated in Supporting Information Figure S1. With this process, MGDs can be fabricated within 30 min. Figure 1B shows the schematic of the experimental setup. A 1.02-k $\Omega$  ballast resistor was connected in series with the MGD to limit the current to elongate the MGD lifetime. A voltage probe (HVP-18HF, PINTEK) was used to monitor the voltage across the MGD. Figure 1C shows the visual appearance of the MGD when the plasma is ignited in the ambient air with a voltage of 2.0 kV and 45 kHz when the ac power source is driven by a 12 V battery. The use of a proper applied voltage is one critical factor for the MGD operation. A test operating the MGD using various applied voltages was performed, and the results were shown in Supporting Information Figure S2. Based on the results, an applied voltage of 2.0 kV is chosen for the MGD operation throughout this work, unless otherwise specified.

**Hydrophobic Paper Substrate.** In this work, three different types of hydrophobized paper were utilized as the paper substrate for the fabrication of  $\mu$ PADs to demonstrate the process viability and flexibility. The first type, fluorocarbon paper, is the filter paper (ADVANTEC grade 2) coated by fluorocarbon utilizing plasma polymerization with a low pressure plasma system. The fluorocarbon plasma polymerization was performed using a parallel-plate capacitively coupled system under the following conditions: c-C<sub>4</sub>F<sub>8</sub> (1 sccm)/Ar (50

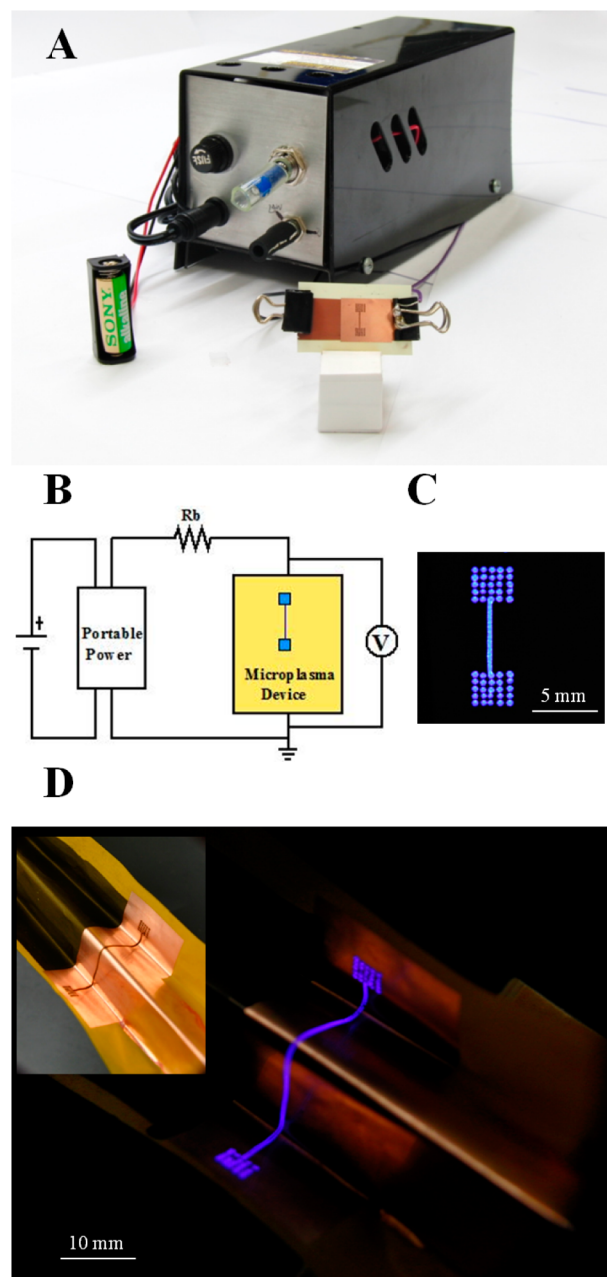


**Figure 1.** (A) Photograph of the experimental setup. (B) Schematic of the experimental setup. (C) Visual appearance of the MGD ignited in the ambient air with a voltage of 2.0 kV and 45 kHz with the power source driven by a 12 V battery. (D) Photograph of a folded MGD with plasma ignited with a voltage of 2.2 kV and 45 kHz. The inset shows the visual appearance of the MGD when plasma is not ignited.

sccm), 13.56 MHz RF power 30 W, and 20 s processing time. The second type of hydrophobized paper, wax paper, is filter paper coated with wax. To prepare this type of hydrophobic paper, filter paper (ADVANTEC grade 2) was dipped in a heptane solution containing paraffin wax (6 g/L) for 10 s and removed and placed in a fume hood to allow evaporation of heptane. The paper samples were then placed on a hot plate at 80 °C for 10 min to cure the wax. The third type of paper, Double A paper, is commercially available copy paper (Double A, 80 gsm). Such a type of paper typically contains internal sizing agents and CaCO<sub>3</sub>, in addition to cellulose. The addition of sizing agents makes the paper fiber hydrophobic and

enhances the paper printability. Alkyl ketene dimer (AKD), for example, is one widely used internal sizing agent in the paper industry. AKD reacts with the hydroxyl functional groups of cellulose and forms a  $\beta$ -keto-ester. These hydrocarbon chains thus impart hydrophobicity to cellulose fiber.<sup>33,34</sup>

**Microfluidic Channels Formation and Channel Shape Examination.** The hydrophilic channels on the above-mentioned hydrophobic paper substrates were fabricated by having the hydrophobized paper face and firmly attach to the surface of the MGD device. The fluorocarbon paper, wax paper, and Double A paper were then treated using the plasma generated on the surface of the MGD with a voltage of 2.0 kV and 45 kHz for 15, 30, and 3 s, respectively, unless otherwise specified. The treatment time for three different kinds of paper is determined experimentally and is the minimal time duration required to pattern a complete hydrophilic channel for fluid flow. The significantly different time durations are due to different hydrophobic material compounds and their amounts (for example, thickness). For example, wax paper has relatively thicker paraffin and requires the longest treatment time to define the hydrophilic channel. Proper selection of the applied voltage and the process time of this MGD-based process is the key to obtain  $\mu$ PADs with desired performance, as demonstrated in Supporting Information Figure S3. For experimental sets to examine the channel shape and width, orange II dye solution was introduced to the hydrophilic channels and the channel shape and width can be clearly visualized. For all tests unless otherwise specified, wax paper was chosen as the hydrophobic paper as the substrate to fabricate  $\mu$ PADs. The microfluidic channel fabricated on wax paper by MGD with an applied voltage of 2.0 kV and 45 kHz for 30 s shows a channel depth of  $56.8 \pm 6.1 \mu\text{m}$ . Such a channel depth together with a typical channel width of  $351.6 \pm 28.6 \mu\text{m}$  yields an aspect ratio (height to width) of 0.16. Given the lateral and vertical diffusion of the reactive species and the limitation of the MGD fabrication process, the smallest trench width that can be fabricated in this process is about  $350 \mu\text{m}$ . The total cost to fabricate  $\mu$ PADs is well below \$USD 0.05/device, including the cost for MGD fabrication, chemicals and materials used, and MGD operation, as detailed in Supporting Information Table S1.

**Chemicals.** The following chemicals were purchased from commercial suppliers (Sigma-Aldrich, Acros) and used as received without further purification: acetone, iron(III) chloride, paraffin wax, *n*-heptane, orange II, D-(+)-glucose, potassium iodide (99.5%), trehalose (98.5%), monosodium phosphate, disodium phosphate, glucose oxidase, horseradish peroxidase, sodium nitrite (99%), *N*-(1-naphthyl)-ethylenediamine (98%), sulfanilamide (99%), and citric acid (99.5%). All aqueous solutions were prepared using deionized water.

**Colorimetric Assays.** In this work, glucose and nitrite assays were tested to confirm that the fabricated  $\mu$ PAD is capable to be used in quantitative analyses. The glucose assay was based on those previously reported.<sup>6,35,36</sup> The glucose indicator was prepared by spotting two solutions on top of the detection region. Solution 1 contains 0.6 M potassium iodide and 0.3 M trehalose in a 100 mM phosphate buffer at pH 6.4. Solution 2 contains 5:1 glucose oxidase (120 units/mL) and horseradish peroxidase (30 units/mL). First, 0.2  $\mu\text{L}$  of solution 1 was applied to the detection region and allowed to dry for 3 min. Then, 0.2  $\mu\text{L}$  of solution 2 was spotted on top of the detection region and allowed to react for another 3 min. Next, 1

$\mu\text{L}$  of D-(+)-glucose solution was added to the sample zone. The  $\mu$ PAD was then placed in a confined humid chamber for 15 min, allowing the enzymes to metabolize the glucose and to form yellow or brown chromogen product. According to Klasner et al.,<sup>35</sup> the humid atmosphere ensures that all channels are wet and thus have enough time for product generation (iodine). Finally, the  $\mu$ PAD was removed out of the humid ambient and allowed to dry at room temperature prior to taking a photo image and scanning.

The  $\text{NO}_2^-$  stock solution was prepared by dissolving sodium nitrite in deionized water. The nitrite indicator contains 10 mM *N*-(1-naphthyl)-ethylenediamine, 50 mM sulfanilamide, and 330 mM citric acid.<sup>37</sup> First, 0.2  $\mu\text{L}$  of the nitrite indicator was spotted in the detection region and allowed to react for 3 min. Then, 1  $\mu\text{L}$  of the nitrite stock solution was spotted on the sample zone. The devices were placed and allowed to dry at room temperature for 5 min before taking the photo image as well as scanning.

**Image Processing.** To quantify the color response, a commercially available scanner (HP, Deskjet F4280 Printer) was used to capture the visual readouts of the colorimetric assays. The scanned image was then deconvoluted using the color image obtained from the detection region into red (R), green (G), and blue (B) components. Two processing schemes using these RGB components were performed to quantify the color image. For the glucose assay, we applied the first scheme, which summarizes the normalized RGB components, as an indicator of the “brightness” of the image. This scheme weighs RGB components equally and is somewhat different from the gray scale, which weighs RGB components differently. As for the nitrite assay, we applied the second scheme, which takes the ratio of  $R/(R+G+B)$  as the quantification, since the colorimetric output produced from the nitrite assay is a red-violet azo compound.<sup>37</sup>

## RESULTS AND DISCUSSION

**Flexibility of the MGD.** Figure 1D shows the visual appearance of the MGD operated in ambient air under a folding configuration. This demonstrates a key feature of the MGD: flexibility. Such a feature allows for treating a curved or nonflat surface; it also extends the nature of this surface treatment process from 2-dimensional to 3-dimensional and offers great possibilities in various applications where treating nonflat surfaces is desired.

**Hydrophilic Trenches on Hydrophobized Paper Substrates.** Making hydrophilic trenches on three types of hydrophobized paper substrates, namely fluorocarbon paper, wax paper, and Double A paper, was demonstrated as the first test in utilization of the MGD-based process to fabricate  $\mu$ PADs. Figure 2A shows the visual appearance of the MGD (upper image) and the plasma generated with this device (lower image) with a specially designed NTUChE-shaped geometry on the MGD. Before MGD treatment, the images with a colored droplet on the surface of three types of hydrophobized paper are shown in the left panel of Figure 2B. It clearly shows the hydrophobic nature with contact angles of 136.9, 124.4, and 108.8° on fluorocarbon paper, wax paper, and Double A paper, respectively. After the hydrophobized paper substrates were treated by MGD, all paper substrates form hydrophilic NTUChE-shaped channels on the surface, as depicted in the right panel of Figure 2B. We note that utilizing Double A paper as the paper substrate for  $\mu$ PADs provides great convenience and opportunities because paper of this type

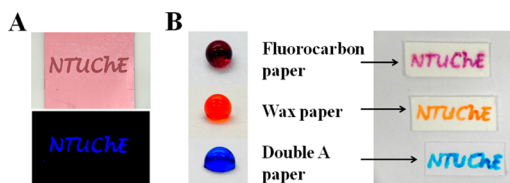


**Figure 2.** (A) Visual appearance of the MGD (upper panel) and the MGD with plasma ignited (lower panel). This MGD is fabricated with a specially designed NTUChE-shaped geometry. (B) Three types of hydrophobized paper: fluorocarbon paper, wax paper, and double A paper before and after treatment with MGD with a voltage of 2.0 kV and 45 kHz for 15, 30, and 3 s, respectively. All paper substrates forming hydrophilic NTUChE-shaped channels on the surface are shown.

is itself hydrophobic and easily accessible and no further hydrophobized process is required.

The plasma ignited by the MGD operated in air is able to generate multiple reactive species, which react with paper substrates, and a substantial increase in surface energy of surfaces occurs.<sup>32</sup> Surfaces with high surface energy are typically more hydrophilic; therefore, hydrophilic microfluidic channels on top of the hydrophobic paper substrates are achieved. Such a plasma treatment process results in surface modification of paper substrates in a designated area without making a visible mark on the treated surface, which retained its flexibility as noted above.

**MGD Pattern-Design and Channel Characteristics.** For this present MGD, plasmas are formed at the edge of the patterns. The area of the paper surface being treated is confined

to the plasma-generated area. To fabricate  $\mu$ PADs with desired channel geometries, a careful design of the MGD is desired. To demonstrate how the geometry of the plasma ignited on the MGD is transferred to the  $\mu$ PADs, MGDs with various geometries were fabricated and corresponding channel shapes were examined. Figure 3 shows 3 sets of tests made by three specially designed patterns. Figure 3A shows the MGD pattern with two 2.5 mm  $\times$  3.0 mm rectangular detection regions connected with a 200  $\mu$ m trench. The image of the plasma ignited on this MGD clearly shows that the plasma “fills” out the trench area while it is confined in the edge of the pattern in the detection zones. When a piece of wax paper is treated using this MGD, the hydrophilic trench can be fabricated as expected. Only the peripheral region of the detection zone becomes hydrophilic. MGD with this pattern is therefore not suitable to make  $\mu$ PADs.

To fabricate a MGD with suitable hydrophilic patterns for the  $\mu$ PAD, a MGD with a 5  $\times$  5 microplasma array with each spot 0.4 mm  $\times$  0.4 mm was designed for the detection region. This device is then used to treat the wax paper to fabricate a  $\mu$ PAD. The plasma visual appearance shown in Figure 3B demonstrates that uniform plasmas are ignited simultaneously in all 50 microcavities. An image with higher magnification is shown in Supporting Information Figure S4. The hydrophilic pattern defined using this MGD is favorable for  $\mu$ PAD detection regions. A further test is performed making channels 200, 400, 600, and 800  $\mu$ m wide on one MGD and using this MGD to fabricate a  $\mu$ PAD. Figure 3C illustrates the results. It clearly shows that, for MGD with trenches 600  $\mu$ m wide or narrower, a well-defined hydrophilic trench can be formed on

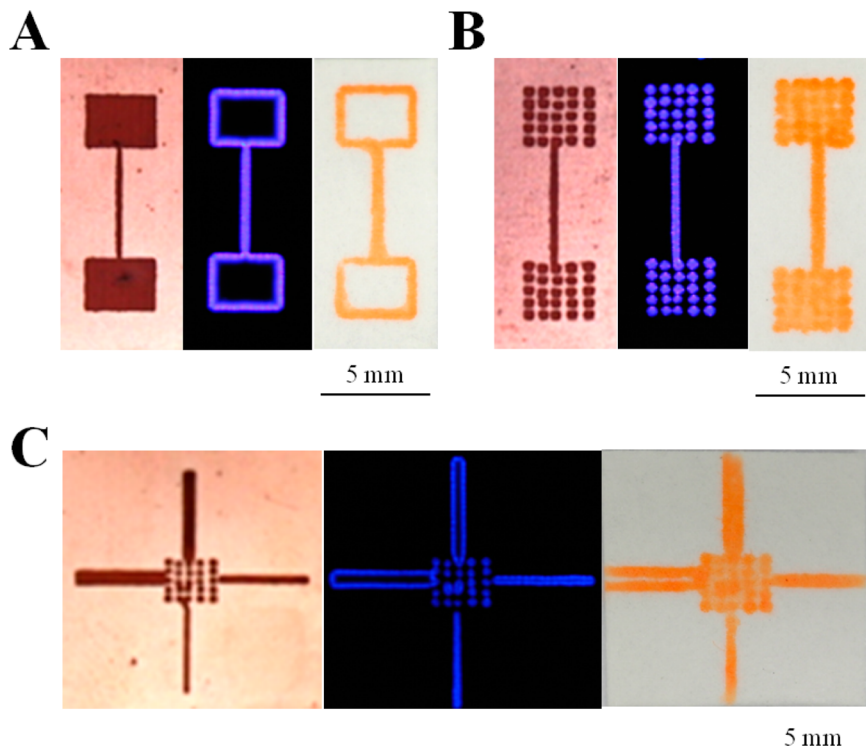


**Figure 3.** Effects of pattern-design on  $\mu$ PAD characteristics. For each set of image, the left, center, and right panels are the visual appearance of the MGD, the MGD with plasma ignited, and the fabricated  $\mu$ PAD, respectively. (A) The MGD pattern with two 2.5 mm  $\times$  3.0 mm rectangular detection regions connected with a 200  $\mu$ m trench. (B) The MGD pattern with two sets of 5  $\times$  5 microplasma arrays with each spot 0.4 mm  $\times$  0.4 mm connected with a 200  $\mu$ m trench. (C) The MGD pattern with one 5  $\times$  5 microplasma array in the middle and four trenches: 200, 400, 600, and 800  $\mu$ m wide.

the wax paper. For MGD with a channel width of 800 micrometer, the hydrophilic channel splits into two. We note that channels 800  $\mu\text{m}$  or wider can be fabricated in a rather straightforward manner by making two or more thinner channels in parallel.

It is shown in this figure that the plasma is not uniform. This is a result of the nonuniformity occurring in both the microscopic and macroscopic scales. In the microscopic scale, such a discharge is filamentary in nature; that is, the discharge consists of a great number of filaments several micrometers wide formed in a time scale of nanoseconds, as reported in the literature.<sup>32</sup> For the nonuniformity in the macroscopic scale, it is caused by the nonuniform thickness of each layer of the CCL as well as the nonideal toner-transfer and etching processes, such as overetch or undercut during the etching step. The nonuniformity in the microscopic scale can be improved by properly adjust the operating condition, particularly using higher frequency or nanosecond pulsed power sources. More precise control in the MGD fabrication process can improve the nonuniformity in the macroscopic scale.

**Assay Tests.** To demonstrate that  $\mu\text{PADs}$  fabricated using the MGD-based process are suitable for quantitative biochemical analyses, we perform glucose and nitrite assays using these  $\mu\text{PADs}$ . Glucose and nitrite assays are both based on the colorimetric sensing mechanism. Detection regions are initially spotted by indicating reagents. After introducing sample solution onto the detection region, a chemical or an enzymatic reaction between the previously immobilized reagents and the sensing target compounds takes place and yields a color change. The glucose assay is based on the enzymatic oxidation of iodide to iodine. It yields a color change from clear to brown. This is one of the most used colorimetric reactions for  $\mu\text{PADs}$  demonstrated reported in the literature. We conduct this assay to demonstrate the practicality of our  $\mu\text{PADs}$ . In Figure 4, images of the glucose assay clearly show different color responses for analytes with different concentrations. The calibration curve shows a linear correlation for the concentration between 1 and 50 mM with an  $R^2$  value of 0.99705.

Nitrite was also chosen as the test assay, since it is a reliable biological marker for many human health conditions, such as periodontal disease.<sup>2</sup> We first applied 0.2  $\mu\text{L}$  of nitrite indicator prior to spotting 1  $\mu\text{L}$  of  $\text{NaNO}_2$  solution with various concentrations onto the sampling zone. The color images of these tested  $\mu\text{PADs}$  are shown in Figure 5. The color responses in the detection regions are reasonably uniform, proving the performance in test solution transportation of our  $\mu\text{PADs}$ . Then, we analyzed the color responses of nitrite assays using image processing scheme II as described in the Experimental Section. The calibration curve shows a linear correlation with the analytes of concentrations between 0.1 and 5 mM with an  $R^2$  value of 0.99706. The performances of glucose and nitrite assays clearly demonstrate that the proposed novel  $\mu\text{PADs}$ -fabricating technique via the MGD-based process is an ideal method to fabricate  $\mu\text{PADs}$  for monitoring people's health conditions.

## CONCLUSION

We report the use of a printed circuit board fabrication-based process to fabricate MGDs in a rapid and cost-effective manner. The MGD can be operated under ambient air and is driven using a portable power source. The use of this MGD to fabricate  $\mu\text{PADs}$  is demonstrated. With a proper design of the MGD electrode geometry,  $\mu\text{PADs}$  with sub-millimeter channel

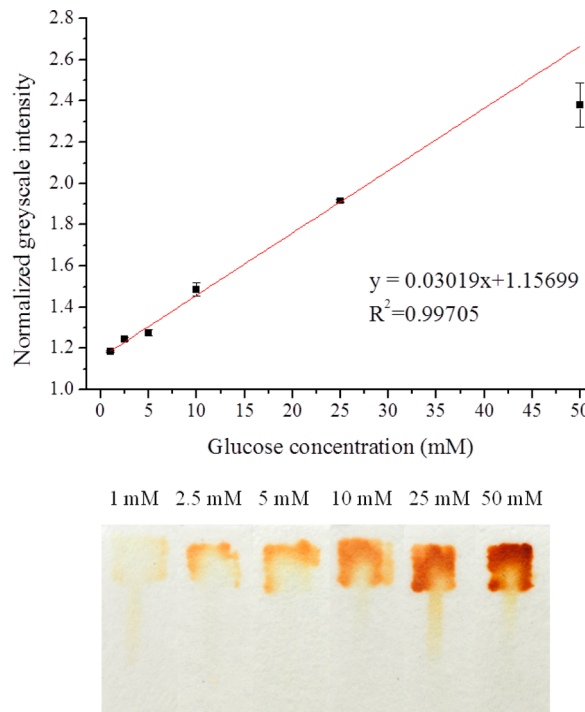


**Figure 4.** Calibration curve for glucose solution using image processing scheme I for color quantification. Color response of glucose assay on the patterned paper for a D-(+)-glucose concentration of 50, 25, 10, 5, 2.5, and 1 mM.

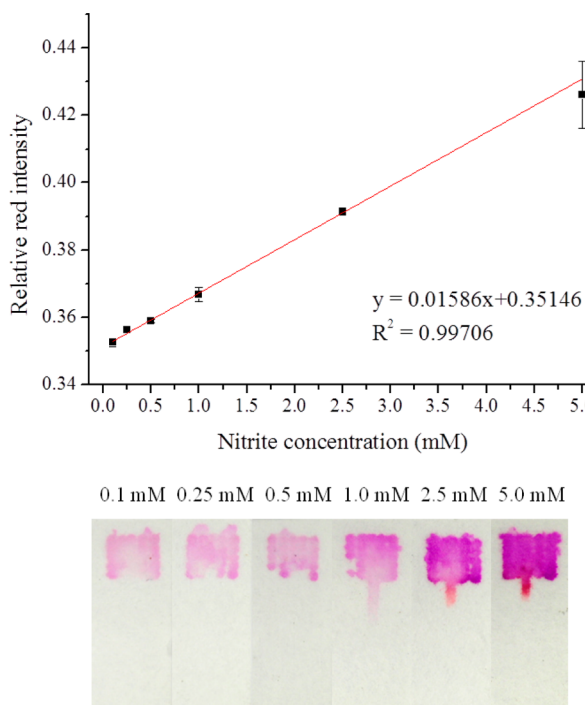


**Figure 5.** Calibration curve for nitrite solution using image processing scheme II for color quantification. Color response of nitrite assay on the patterned paper for  $\text{NaNO}_2$  concentrations of 5, 2.5, 1, 0.5, 0.25, and 0.1 mM.

width can be fabricated within 1 min and with a total cost less than \$USD 0.05/device. This MGD possesses great flexibility, which could be a benefit for treating curved or nonflat surfaces. It could also extend the nature of this surface treatment process

from 2-dimensional to 3-dimensional and offers great possibilities for surfaces with various orientations. We also demonstrate that three types of hydrophobized paper, fluorocarbon paper, wax paper, and Double A paper, can be treated by MGD and form microfluidic channels in the paper platforms. We further investigate the relationship between MGD pattern-design and channel characteristics. The MGD pattern with two sets of  $5 \times 5$  microplosma arrays with each spot  $0.4 \text{ mm} \times 0.4 \text{ mm}$  connected with a  $200\text{-}\mu\text{m}$ -wide trench was designed and was selected to fabricate our  $\mu$ PADs. Finally, we tested the  $\mu$ PADs by performing quantitative colorimetric assay tests and established calibration curves for detecting glucose and nitrite.

The cost-effective and portable features of the MGD make this MGD-based process a great candidate to fabricate  $\mu$ PADs in-field and/or on demand. The demonstration driving the MGD using a 12 V battery offers great possibilities under circumstances when  $\mu$ PADs are required to be fabricated in locations where stable electricity is not available. A great number of commercially available batteries deliver dc 12 V, such as lead-acid rechargeable batteries for automobiles. A typical battery of this type with a capacity of 45 amp-hour is sufficient to supply the MGD operation for at least 20 h. We believe this concept brings a leap to the fabrication and use of the impact of  $\mu$ PADs, which gives great impact in various applications, such as biomedical analysis, environmental monitoring, and food safety survey.

## ■ ASSOCIATED CONTENT

### S Supporting Information

Additional information as noted in text. This material is available free of charge via the Internet at <http://pubs.acs.org/>.

## ■ AUTHOR INFORMATION

### Corresponding Author

\*E-mail: chsu@ntu.edu.tw.

### Notes

The authors declare no competing financial interest.

## ■ ACKNOWLEDGMENTS

This work is supported by the Ministry of Science and Technology, Taiwan (101-2221-E-002-163-MY2).

## ■ REFERENCES

- (1) Hsu, M. Y.; Yang, C. Y.; Hsu, W. H.; Lin, K. H.; Wang, C. Y.; Shen, Y. C.; Chen, Y. C.; Chau, S. F.; Tsai, H. Y.; Cheng, C. M. *Biomaterials* **2014**, *35*, 3729–3735.
- (2) Bhakta, S. A.; Borba, R.; Taba, M.; Garcia, C. D.; Carrilho, E. *Anal. Chim. Acta* **2014**, *809*, 117–122.
- (3) Hsu, C.-K.; Huang, H.-Y.; Chen, W.-R.; Nishie, W.; Ujiie, H.; Natsuga, K.; Fan, S.-T.; Wang, H.-K.; Lee, J. Y.-Y.; Tsai, W.-L.; Shimizu, H.; Cheng, C.-M. *Anal. Chem.* **2014**, *86*, 4605–4610.
- (4) Lo, S. J.; Yang, S. C.; Yao, D. J.; Chen, J. H.; Tu, W. C.; Cheng, C. M. *Lab Chip* **2013**, *13*, 2686–2692.
- (5) Cheng, C. M.; Martinez, A. W.; Gong, J. L.; Mace, C. R.; Phillips, S. T.; Carrilho, E.; Mirica, K. A.; Whitesides, G. M. *Angew. Chem., Int. Ed.* **2010**, *49*, 4771–4774.
- (6) Martinez, A. W.; Phillips, S. T.; Butte, M. J.; Whitesides, G. M. *Angew. Chem., Int. Ed.* **2007**, *46*, 1318–1320.
- (7) Mentele, M. M.; Cunningham, J.; Koehler, K.; Volckens, J.; Henry, C. S. *Anal. Chem.* **2012**, *84*, 4474–4480.
- (8) Rattanarat, P.; Dungchai, W.; Cate, D.; Volckens, J.; Chailapakul, O.; Henry, C. S. *Anal. Chem.* **2014**, *86*, 3555–3562.
- (9) Hossain, S. M. Z.; Luckham, R. E.; McFadden, M. J.; Brennan, J. D. *Anal. Chem.* **2009**, *81*, 9055–9064.
- (10) Yetisen, A. K.; Akram, M. S.; Lowe, C. R. *Lab Chip* **2013**, *13*, 2210–2251.
- (11) Li, X.; Tian, J.; Nguyen, T.; Shen, W. *Anal. Chem.* **2008**, *80*, 9131–9134.
- (12) Kao, P.-K.; Hsu, C.-C. *Microfluid Nanofluid* **2014**, *16*, 811–818.
- (13) Carrilho, E.; Martinez, A. W.; Whitesides, G. M. *Anal. Chem.* **2009**, *81*, 7091–7095.
- (14) Zhang, Y.; Zhou, C. B.; Nie, J. F.; Le, S. W.; Qin, Q.; Liu, F.; Li, Y. P.; Li, J. P. *Anal. Chem.* **2014**, *86*, 2005–2012.
- (15) Abe, K.; Suzuki, K.; Citterio, D. *Anal. Chem.* **2008**, *80*, 6928–6934.
- (16) Cheng, C. M.; Mazzeo, A. D.; Gong, J. L.; Martinez, A. W.; Phillips, S. T.; Jain, N.; Whitesides, G. M. *Lab Chip* **2010**, *10*, 3201–3205.
- (17) Olkkonen, J.; Lehtinen, K.; Erho, T. *Anal. Chem.* **2010**, *82*, 10246–10250.
- (18) Bruzewicz, D. A.; Reches, M.; Whitesides, G. M. *Anal. Chem.* **2008**, *80*, 3387–3392.
- (19) Cassano, C. L.; Fan, Z. H. *Microfluid Nanofluid* **2013**, *15*, 173–181.
- (20) Liu, H.; Crooks, R. M. *Anal. Chem.* **2012**, *84*, 2528–2532.
- (21) Kakei, R.; Ogino, A.; Iwata, F.; Nagatsu, M. *Thin Solid Films* **2010**, *518*, 3457–3460.
- (22) Becker, K. H.; Schoenbach, K. H.; Eden, J. G. *J. Phys. D: Appl. Phys.* **2006**, *39*, R55–R70.
- (23) Szili, E. J.; Al-Bataineh, S. A.; Ruschitzka, P.; Desmet, G.; Priest, C.; Griesser, H. J.; Voelcker, N. H.; Harding, F. J.; Steele, D. A.; Short, R. D. *RSC Adv.* **2012**, *2*, 12007–12010.
- (24) Yang, Y. J.; Hsu, C. C. *J. Microelectromech. Syst.* **2013**, *22*, 256–258.
- (25) Kim, S. J.; Chung, T. H.; Bae, S. H.; Leem, S. H. *Appl. Phys. Lett.* **2009**, *94*, 141502.
- (26) Symonds, J. M.; Galhena, A. S.; Fernandez, F. M.; Orlando, T. M. *Anal. Chem.* **2010**, *82*, 621–627.
- (27) Weagant, S.; Chen, V.; Karanassios, V. *Anal. Bioanal. Chem.* **2011**, *401*, 2865–2880.
- (28) Hsu, C. C.; Tsai, J. H.; Yang, Y. J.; Liao, Y. C.; Lu, Y. W. *J. Microelectromech. Syst.* **2012**, *21*, 1013–1015.
- (29) Tachibana, K. *IEE J. Trans. Electrical Electronic Eng.* **2006**, *1*, 145–155.
- (30) Karanassios, V. *Spectrochim. Acta, Part B: At. Spectrosc.* **2004**, *59*, 909–928.
- (31) Gibalov, V. I.; Pietsch, G. J. *J. Phys. D: Appl. Phys.* **2000**, *33*, 2618–2636.
- (32) Kogelschatz, U. *Plasma Chem. Plasma Process.* **2003**, *23*, 1–46.
- (33) Garnier, G.; Wright, J.; Godbout, L.; Yu, L. *Colloids Surf., A* **1998**, *145*, 153–165.
- (34) Li, X.; Tian, J.; Shen, W. *Cellulose* **2010**, *17*, 649–659.
- (35) Klasner, S. A.; Price, A. K.; Hoeman, K. W.; Wilson, R. S.; Bell, K. J.; Culbertson, C. T. *Anal. Bioanal. Chem.* **2010**, *397*, 1821–1829.
- (36) Martinez, A. W.; Phillips, S. T.; Carrilho, E.; Thomas, S. W.; Sindi, H.; Whitesides, G. M. *Anal. Chem.* **2008**, *80*, 3699–3707.
- (37) Blicharz, T. M.; Rissin, D. M.; Bowden, M.; Hayman, R. B.; DiCesare, C.; Bhatia, J. S.; Grand-Pierre, N.; Siqueira, W. L.; Helmerhorst, E. J.; Loscalzo, J.; Oppenheim, F. G.; Walt, D. R. *Clin. Chem.* **2008**, *54*, 1473–1480.